DSEC-Aware: Post-Collision Safety Control of Mobile Manipulators via Directional Energy Constraints

Jinhua Ye, *Senior Member, IEEE*, Yechen Fan, *Graduate Student Member, IEEE*, Linxin Hong, Haibin Wu, and Gengfeng Zheng, *Senior Member, IEEE*

***Abstract*—In this letter, we introduce a Directionally-aware Dynamic Energy Constraint (DSEC-Aware) framework to enhance energy-based safety control in post-collision human-robot collaboration (HRC). The method employs a selective energy dissipation mechanism, applying variable damping only along critical collision directions to effectively reduce impact forces while preserving user motion intentions in non-critical directions. It further adjusts energy boundaries dynamically according to human-robot proximity and introduces a multidimensional Danger Index (DI) model that incorporates physical parameters such as effective mass, contact stiffness, and human tolerance limits for accurate risk evaluation. Experimental results demonstrate that, compared with state-of-the-art (SOTA) methods, the proposed strategy reduces collision forces by approximately 58.04% and consistently maintains a low and stable collision risk, thereby significantly improving both the safety and practicality of HRC.**

***Index Terms*—Human-robot collaboration, compliance control, post-collision safety control, variable damping, danger index model.**

I. Introduction

The complexity of HRC is increasing, making it a critical challenge to ensure safe and efficient collaboration within shared workspaces [1]. This is especially true in dynamic environments involving mobile manipulators, where accidental collisions with operators are difficult to completely avoid. Therefore, accurately assessing the risk following a collision and effectively controlling the robot to reduce impact force are central issues in enhancing the safety of physical human-robot interaction. In this context, "safety" refers to maintaining collision forces and energies within the human tolerance limits specified by ISO/TS 15066 [21].

Although compliance control has made progress in absorbing contact energy through passive and active means [2], [3], and some studies have addressed potential collision energy, existing methods remain limited in mitigating impact forces once collisions occur. Even rigorous approaches such as Control Barrier Functions (CBFs) [27] rely on geometric constraints as proxies for impact forces, overlooking critical dynamics such as configuration-dependent effective mass [28]. These limitations are especially pronounced in mobile manipulators with complex inertial effects. Moreover, fixed passive parameters cannot adapt to varying collision energies, while active compliance methods are vulnerable to model mismatches and often employ global damping, which unnecessarily restricts user motion, degrades force control, and fails to dynamically adjust safety parameters.

Meanwhile, current collision risk assessment methods lack a comprehensive consideration of key physical factors. Most existing studies [5], [12] rely on kinematic parameters, neglecting effective collision mass, contact stiffness, collision posture, and the varying damage thresholds of different human body parts. This results in biased and inaccurate risk assessments that cannot support optimal compliance strategies. This interdependence creates a crucial bottleneck, as any impact mitigation strategy is rendered ineffective without a robust risk assessment to guide it.

To address these challenges, this letter proposes the DSEC-Aware framework, a novel approach that directly focuses on the physical realities of post-collision events (see Fig. 1). To move beyond indirect geometric proxies, the framework first constrains the robot's directional kinetic energy, a quantity that is not only directly correlated with impact severity but also incorporates configuration-dependent effective mass. This energy is bounded within an adaptive energy boundary that dynamically adjusts according to human-robot proximity. To satisfy this boundary while avoiding the drawbacks of indiscriminate global damping, a selective energy dissipation mechanism is constructed, applying optimal variable damping only along critical collision directions to preserve user motion intentions. Finally, to enable comprehensive risk evaluation, a multidimensional DI is established, integrating effective mass, contact stiffness, and

Received 25 June 2025; accepted 30 September 2025. Date of publication 15 October 2025; date of current version 23 October 2025. This article was recommended for publication by Associate Editor R. Qi and Editor C. D. Santina upon evaluation of the reviewers' comments. This work was supported in part by the Projects of Fujian University Industry-Academic Cooperation under Grant 2022H6016, in part by the Collaborative Education Project of the Ministry of Education under Grant 231003084265411, in part by the Talent Program of the State Administration for Market Regulation under Grant QNBJ202319, and in part by the Research project of Fujian Provincial Market Supervision Bureau under Grant FJMS2023016. *(Corresponding author: Gengfeng Zheng.)*

Jinhua Ye, Yechen Fan, Linxin Hong, and Haibin Wu are with the School of Mechanical Engineering and Automation, Fuzhou University, Fuzhou 350116, China (e-mail: yejinhua@fzu.edu.cn).

Gengfeng Zheng is with the Fujian Key Laboratory of Special Intelligent Equipment Safety Measurement and Control, Fujian Special Equipment Inspection and Research Institute, Fuzhou 350008, China (e-mail: 18862889747@163.com).

Digital Object Identifier 10.1109/LRA.2025.3621933

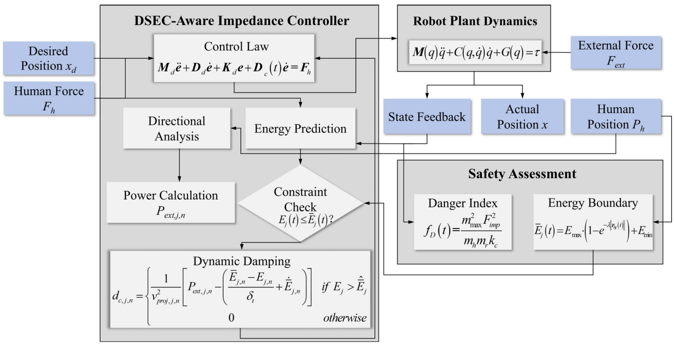

Fig. 1. Overall Framework of the DSEC-Aware Strategy. The diagram illustrates an active safety control system that dynamically adjusts damping to keep the robot's kinetic energy within safe boundaries, complemented by an independent hazard index to assess the severity of potential collisions.

human tolerance data to provide a physically grounded and more accurate assessment.

In summary, our main contributions are as follows:

- A direction-aware dynamic energy constraint method is proposed to reduce post-collision impact forces.
- An energy boundary curve based on human-robot distance is designed to achieve precise limitation of collision energy.
- A Danger Index model is constructed to enable accurate and multidimensional risk control.

II. Related Works

A. Active/Passive Compliance Control

Robot compliance control enhances HRC safety and adaptability, particularly after collisions. Passive compliance absorbs impacts via elastic elements [5], [6], with designs such as compliant mechanisms to reduce force fluctuations [7] and Series Elastic Actuators (SEA) for flexible collaboration [8]. However, fixed stiffness cannot adapt to dynamic collisions, and even Variable Stiffness Actuators (VSA) remain limited for sudden impacts [9]. Active and hybrid compliance provide more precise force/position control, often combined with passive elements [10], [11]; examples include online adaptation [12], reduced impacts on mobile platforms [13], and robust control for flexible joints [14]. Nevertheless, active control of complex mobile robots still lacks effective collision energy constraint and distance-based parameter adaptation, making highly dynamic scenarios difficult to manage.

B. Risk Assessment and Energy Management

Recent studies on HRC safety mainly focus on risk assessment and energy management. For risk assessment, injury indices based on dissipated kinetic energy [15] and viscoelastic models of human soft tissues [16] have been used to determine safe robot speed and mass. Improved models incorporate velocity and indirect factors [17], acceleration-based discriminators [18], and even deep learning for terrain traversability and stereo vision-based risk estimation [19]. For energy management, bounded-energy strategies using variable damping, stored energy limitation [20], joint-space damping injection [4], and Hamiltonian energy-flow regulation [5] have been proposed. However, these methods still lack adaptability and robustness in multidimensional risk modeling, collision directionality, and injury assessment, limiting their real-world applicability.

III. Methodology

To clearly illustrate the DSEC-Aware strategy, Fig. 2 provides an overview.

A. Theoretical Foundation of DSEC-Aware Control

Theorem 1 (Directional Energy Constraint)): For a robotic system in contact with a human operator, the maximum impact force $F_{\text{imp},j}$ in any direction j is bounded by:

$$F_{\text{imp},j} \leq \sqrt{2k_c m_{\text{eff},j} E_j}$$

where k_c represents contact stiffness, $m_{\text{eff},j}$ is the effective mass in direction j, and E_j is the directional kinetic energy.

This relationship derives from energy conservation during collision ($E_j = \frac{1}{2}k_c x_{\max}^2$) and Hooke's law ($F_{\text{imp},j} = k_c x_{\max}$), where the directional kinetic energy E_j determines the stored elastic energy and thus the peak contact force. By directly constraining E_j, our approach controls the physical quantity that generates impact forces, establishing the theoretical foundation for directional energy constraint.

Corollary 1: If the directional energy constraint $E_j(t) \leq \bar{E}_j(t)$ is maintained for all critical directions j, then the impact forces remain within physiologically acceptable limits, provided $\bar{E}_j(t)$ is designed based on human tolerance data.

This theoretical foundation distinguishes our approach from established methods. While CBFs enforce geometric safety via a condition like $h(\boldsymbol{x}) \geq 0$, our theory ensures physical safety by directly constraining energy states that govern the underlying collision mechanics.

B. Directionally-Aware Energy-Constrained Impedance Control

The main objective of the DSEC-Aware impedance controller is to constrain the system's energy within a safe range during collisions by dynamically adjusting its damping parameters. The robot impedance control model is given as follows [5]:

$$\mathbf{M}_d\ddot{\mathbf{e}} + \mathbf{D}_d\dot{\mathbf{e}} + \mathbf{K}_d\mathbf{e} + \mathbf{D}_c(t)\dot{\mathbf{e}} = \mathbf{F}_h \tag{1}$$

where $\mathbf{e} \in \mathbb{R}^6$ represents the six-dimensional pose error of the robot's end-effector in task space. $\dot{\mathbf{e}}$ and $\ddot{\mathbf{e}}$ denote the velocity and acceleration errors, respectively. $\mathbf{M}_d, \mathbf{D}_d, \mathbf{K}_d \in \mathbb{R}^{6\times 6}$ are the desired inertia, damping, and stiffness positive definite matrices of the robot. $\mathbf{F}_h \in \mathbb{R}^6$ denotes the external contact force vector. The core of our work lies in the design of the time-varying damping matrix $\mathbf{D}_c(t) \in \mathbb{R}^{6\times 6}$.

To clarify the core idea of the DSEC-Aware strategy, we first simplify the complex system into a single-degree-of-freedom model for analysis. This simplified model satisfies the following:

$$m_d\ddot{e} + d_d\dot{e} + k_d e + d_c(t)\dot{e} = f_h \tag{2}$$

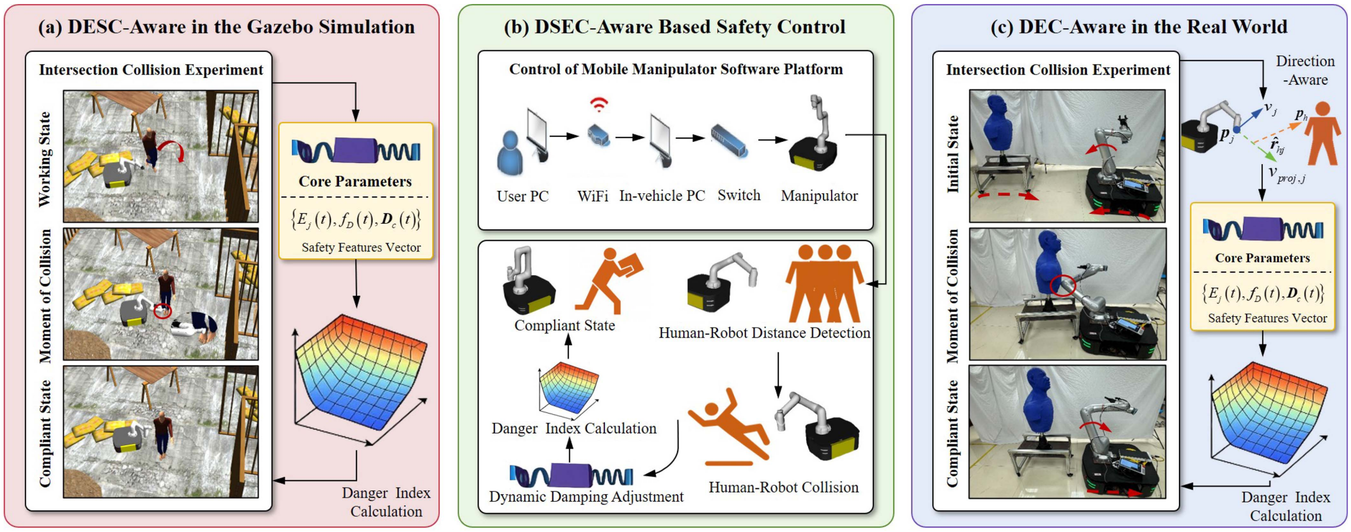

Fig. 2. Overview of the DSEC-Aware Strategy. (a) The core DSEC-Aware is validated in a Gazebo simulation environment, demonstrating direction-aware compliance and risk assessment. (b) The control architecture for the real-world system, which processes human-robot distance and collision data to dynamically adjust damping. (c) The DSEC-Aware Strategy is deployed on a real mobile robotic arm, showing its effectiveness in a real-world intersection collision experiment.

where m_d, d_d and k_d denote the system's equivalent mass, damping, and stiffness, respectively. f_h represents the external force, while $d_c(t)$ is the time-varying damping term that we design.

To predict the system's energy state at the next time step, we apply a first-order Taylor expansion [12] to the system's kinetic energy. In discrete-time systems, the kinetic energy at the next time step, E_{n+1}, can be approximated as:

$$E_{n+1} \approx E_n + \dot{E}_n \delta t \tag{3}$$

where E_n represents the current kinetic energy, $\dot{E}_n$ denotes its time derivative, δt represents the sampling interval. Similarly, the estimated kinetic energy boundary $\bar{E}_{n+1}$ at the next time step can be expressed as:

$$\bar{E}_{n+1} = \bar{E}(\boldsymbol{x}_n + \dot{\boldsymbol{x}}_n\, \delta t) \approx \bar{E}_n + \dot{\bar{E}}_n\, \delta t \tag{4}$$

Conventional global damping methods often interfere unnecessarily with the user's intended motions, even in directions that pose no safety risks. To address this limitation, we extend our core concept into a multi-dimensional space and introduce directional analysis to enable more precise and responsive control.

To this end, we first identify potential collision boundaries around the robot. We model each robot link with a set of key geometric primitives and determine the closest boundary point, $\mathbf{p}_j \in \mathbb{R}^3$ relative to a given body part of the human operator. The unit vector $\hat{\mathbf{r}}_{hj}$, indicating the direction of potential collision from the robot's boundary point $\mathbf{p}_j$ towards the human operator's point $\mathbf{p}_h$, is defined as:

$$\hat{\boldsymbol{r}}_{hj} = \frac{\mathbf{p}_h - \mathbf{p}_j}{||\mathbf{p}_h - \mathbf{p}_j||} \tag{5}$$

where $\mathbf{p}_h \in \mathbb{R}^3$ refers to the point on the operator's body that is closest to the robot. In the computation, we use their positions represented as vectors in the world coordinate frame. Both vectors belong to $\mathbb{R}^3$, and their difference $(\mathbf{p}_h - \mathbf{p}_j)$ yields a vector pointing from $\mathbf{p}_j$ to $\mathbf{p}_h$.

Next, we project the robot's motion onto this critical direction. The velocity $\mathbf{v}_j$ of point $\mathbf{p}_j$ in Cartesian space can be obtained using its positional Jacobian $\mathbf{J}_j(\mathbf{q})$ and the joint velocity $\dot{\mathbf{q}}$, as follows [23]:

$$\mathbf{v}_j = \mathbf{J}_j(\mathbf{q})\dot{\mathbf{q}} \tag{6}$$

where $\mathbf{q} \in \mathbb{R}^n$ represents the joint angle vector of the robot. Therefore, the velocity projected along the boundary direction, denoted as $v_{\text{proj},j}$, is given by:

$$v_{\text{proj},j} = \mathbf{v}_j^T \hat{\boldsymbol{r}}_{hj} = (\mathbf{J}_j(\mathbf{q})\dot{\mathbf{q}})^T \hat{\boldsymbol{r}}_{hj} \tag{7}$$

To quantify the kinetic energy along this direction, we define the effective mass $m_{\text{eff},j}$ of the robot in the given direction as [24]:

$$m_{\text{eff},j} = (\hat{\boldsymbol{r}}_{hj}^T \mathbf{J}_j(\mathbf{q}) \mathbf{M}_q(\mathbf{q})^{-1} \mathbf{J}_j^T(\mathbf{q}) \hat{\boldsymbol{r}}_{hj})^{-1} \tag{8}$$

where $\mathbf{M}_q(\mathbf{q}) \in \mathbb{R}^{n\times n}$ denotes the robot's mass matrix in joint space. Accordingly, the actual kinetic energy E_j of the system along this direction can be computed as:

$$E_j = \frac{1}{2} m_{\text{eff},j} v_{\text{proj},j}^2 \tag{9}$$

For each direction, we define a safety kinetic energy boundary $\bar{E}_j(t)$ that dynamically varies with the distance $||\mathbf{r}_{hj}||$ [26]:

$$\bar{E}_j(t) = E_{\max} \cdot (1 - e^{-\lambda ||\mathbf{r}_{hj}(t)||}) + E_{\min} \tag{10}$$

where $E_{\max}$ and $E_{\min}$ represent the maximum and minimum allowable kinetic energies, respectively, and λ denotes the decay rate.

This distance-dependent energy boundary is analogous to the class-K function in CBF theory [27], which tightens constraints near boundaries. Unlike geometric functions, however, our formulation directly constrains kinetic energy, aligning safety control with the physical goal of impact force mitigation.

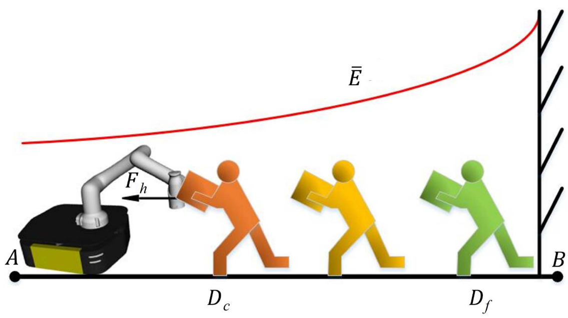

Fig. 3. Variation of Collision Energy Constraint Based on Hazard Index.

TABLE I
PHYSICAL PARAMETERS AND SAFETY LIMITS FOR BODY REGIONS

Region	Shore Hardness	Stiffness Coefficient k_c (N/mm)	Effective Mass m_h (kg)	Impact Force F (N)	Pressure P (N/cm^2)
Forehead	70	150	4.4	130	110
Face	70	75	4.4	65	110
Forearm	70	40	2	160∼320	180∼360
Hand	70	75	0.6	140∼280	190∼380

The goal of the DSEC-Aware strategy is to ensure that, at any time t and in any critical direction j, the following energy constraint is always satisfied:

$$E_j(t) \leq \bar{E}_j(t) \tag{11}$$

In a discrete-time system, to ensure that the energy constraint $E_{j,n+1}(t) \leq \bar{E}_{j,n+1}(t)$ is satisfied at the next time step $n+1$, we apply a first-order Taylor expansion to both the kinetic energy and its boundary:

$$E_{j,n+1}(t) \approx E_{j,n} + \dot{E}_{j,n}\delta t \tag{12}$$

$$\bar{E}_{j,n+1}(t) \approx \bar{E}_{j,n} + \dot{\bar{E}}_{j,n}\delta t \tag{13}$$

By substituting equations (12) and (13) into the energy constraint condition (11), we derive the required condition on the kinetic energy rate $\dot{E}_{j,n}$ of change at the current time step:

$$\dot{E}_{j,n} \leq \frac{\bar{E}_{j,n} - E_{j,n}}{\delta t} + \dot{\bar{E}}_{j,n} \tag{14}$$

According to the principle of power balance, the rate $\dot{E}_j$ of change of kinetic energy in a one-dimensional directional system is equal to the total power exerted by all forces along that direction. Let $P_{\text{total},j}$ denote the total power; then:

$$\dot{E}_j = P_{\text{total},j} = P_{\text{ext},j} - P_{\text{damp},j} \tag{15}$$

where $P_{\text{ext},j}$ represents the power generated along the direction by all forces *apart from* the additional damping—this includes external forces, inherent damping forces, stiffness forces, etc. $P_{\text{damp},j}$ denotes the dissipative power produced by the scalar additional damping $d_{c,j}$, which we aim to determine:

$$P_{\text{damp},j} = d_{c,j} v_{\text{proj},j}^2 \tag{16}$$

By substituting equations (15) and (16) into (14), we obtain:

$$P_{\text{ext},j} - d_{c,j,n} v_{\text{proj},j,n}^2 \leq \frac{\bar{E}_{j,n} - E_{j,n}}{\delta t} + \dot{\bar{E}}_{j,n} \tag{17}$$

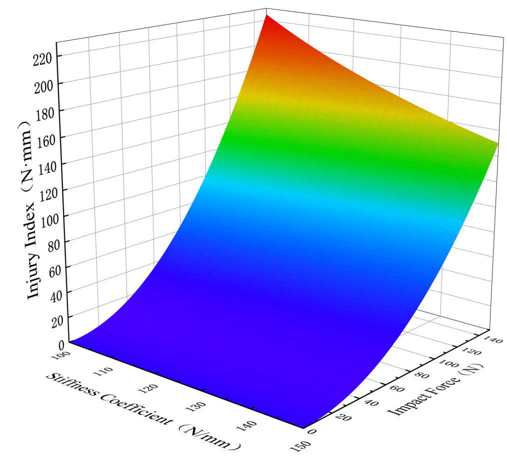

Fig. 4. Variation of the Danger Index in HRC.

Equation (17) represents a fundamental energy balance constraint for ensuring collision safety, leading to our central control-theoretic contribution: when the predicted energy is about to exceed the limit, a scalar additional damping $d_{c,j}$ must be computed and applied to dissipate the excess energy and satisfy the constraint.

To satisfy this inequality, we derive the optimal damping value as stated in the following theorem.

Theorem 2 (Minimally Invasive Damping Law): The damping value $d_{c,j,n}$ is given by

$$d_{c,j,n} = \begin{cases} \frac{1}{v_{\text{proj},j,n}^2}\left(P_{\text{ext},j,n} + \frac{E_{j,n} - \bar{E}_{j,n}}{\delta t} - \dot{\bar{E}}_{j,n}\right) & \text{if } E_j > \bar{E}_j \\ 0 & \text{otherwise} \end{cases} \tag{18}$$

This law provides the optimal analytical solution to the formal optimization problem of finding the minimum control effort subject to the safety constraint:

$$d_{c,j,n}^* = \arg\min_{d_{c,j,n} \geq 0} d_{c,j,n} \quad \text{s.t.} \quad E_{j,n+1} \leq \bar{E}_{j,n+1}$$

The analytical solution, derived via the Karush-Kuhn-Tucker (KKT) conditions, corresponds directly to (18).

Finally, to integrate the damping requirements across all directional components, we construct the additional damping $\mathbf{D}_c(t)$ as follows:

$$\mathbf{D}_c(t) = \sum_j d_{c,j}(t)\hat{\boldsymbol{r}}_{hj}(t)\hat{\boldsymbol{r}}_{hj}(t)^T \tag{19}$$

In (19), the summation $\sum_j$ iterates over all monitored critical points. Each term $\hat{\boldsymbol{r}}_{hj}(t)\hat{\boldsymbol{r}}_{hj}(t)^T$ denotes a rank-one matrix that confines the effect of the scalar damping $d_{c,j}(t)$ strictly to the direction $\hat{\boldsymbol{r}}_{hj}(t)$. The resulting matrix, $\mathbf{D}_c(t)$, is symmetric and positive semi-definite, providing the exact amount of damping required in each critical direction while minimizing damping in non-critical directions.

This design preserves the robot's intended impedance as long as E_j stays within the safety boundary $\bar{E}_j$. When a violation is imminent, (18) adjusts damping according to the distance-dependent boundary in (10), ensuring safety. As shown in Fig. 3,

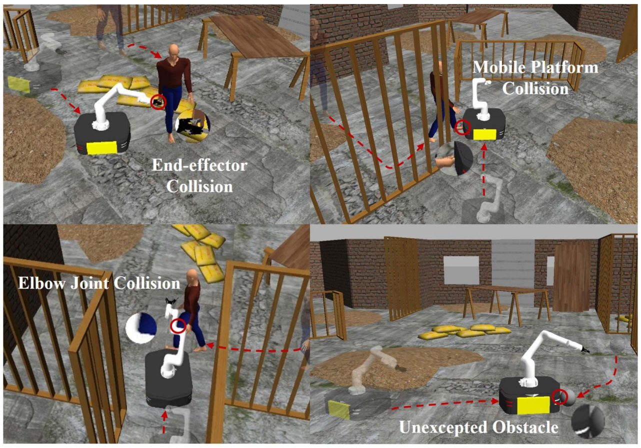

Fig. 5. Gazebo Simulation Scenarios. The four simulation scenarios cover collisions with the end-effector, elbow joint, mobile base, and an unexpected obstacle to ensure comprehensive validation.

TABLE II
QUANTITATIVE COMPARISON OF SIMULATION RESULTS ACROSS DIFFERENT CONTROLLERS

Scenarios	Trial	FI	BEC	DSEC-Aware (Ours)	Improvement over BEC
End-effector Collision	30	175.2±15.3	95.8±8.1	40.1±2.5	58.1%
Elbow Joint Collision	30	190.4±18.9	105.1±9.7	45.3±3.1	56.9%
Platform Collision	30	250.1±25.1	140.6±15.2	62.5±5.4	55.5%
Unexpected Obstacle	30	165.7±14.5	90.3±7.8	38.6±2.9	57.3%

$\bar{E}_j$ decreases smoothly with human-robot distance, and damping increases once the boundary is exceeded to enforce the energy constraint.

C. Human-Robot Collision Risk Quantification Via Danger Index

Building on the DSEC-Aware strategy's ability to ensure energy controllability, the DI model quantifies collision severity through the physical mechanism of impact force generation, using a spring-mass formulation that simplifies the collision process as the conversion of relative kinetic energy into elastic potential energy at the contact interface, where, by energy conservation, all relative kinetic energy is fully transformed into elastic potential energy [25].

$$\frac{1}{2}\mu v_{\text{rel}}^2 = \frac{1}{2}k_c x_{\max}^2 \tag{20}$$

where v_{rel} represents the relative velocity between the human and the robot before the collision, k_c represents the equivalent stiffness of the human-robot contact. and $x_{\max}$ denotes the maximum compression deformation. The equivalent mass μ of the human-robot system is defined as $\mu = (m_h^{-1} + m_r^{-1})^{-1}$, where m_h and m_r represent the effective mass of the human and the robot in the collision direction, respectively.

According to Hooke's law, the maximum impact force F_{imp} is related to the maximum compression $x_{\max}$ by $F_{\text{imp}} = k_c x_{\max}$. Therefore, the impact force can be expressed as:

$$F_{\text{imp}} = v_{\text{rel}}\sqrt{k_c \mu} \tag{21}$$

To compute the impact force, it is necessary to determine the robot's effective mass in the direction of collision [24], denoted as m_r:

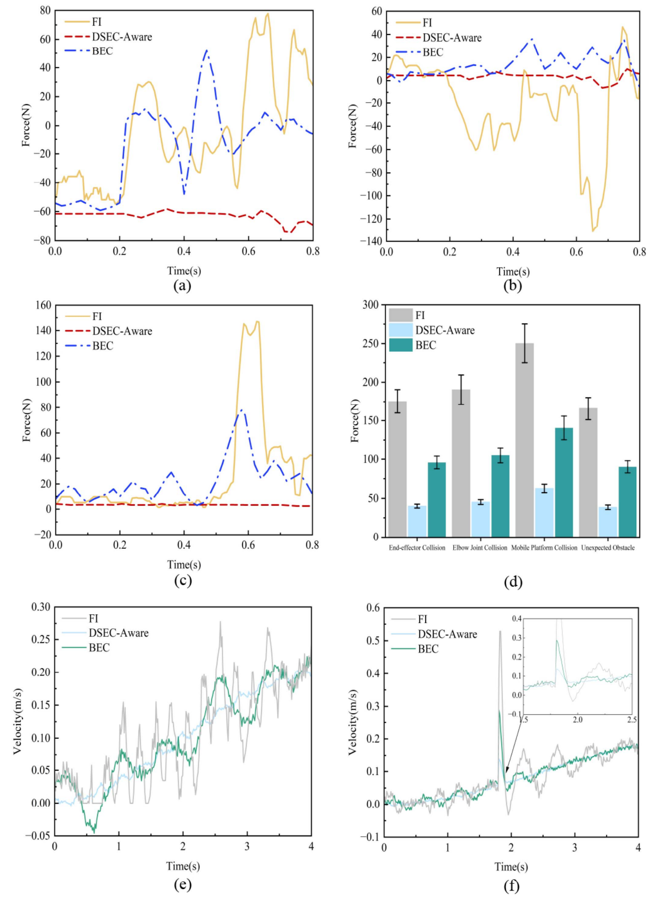

Fig. 6. Performance comparison of different control strategies in simulation. (a–c) Force–time curves for collisions involving the end-effector, elbow joint, and mobile platform, respectively. (d) Statistical comparison of peak collision forces across four scenarios. (e–f) Velocity–time curves of the two front wheels in the mobile platform collision scenario.

$$m_r = \{\mathbf{u}^T[\mathbf{J}(\mathbf{q})\mathbf{M}(\mathbf{q})^{-1}\mathbf{J}^T(\mathbf{q})]\mathbf{u}\}^{-1} \tag{22}$$

where $\mathbf{u}$ denotes the unit vector in the direction of the collision. By substituting (22) into (21), we obtain a more specific expression for the impact force as:

$$F_{\text{imp}} = v_{\text{rel}}\sqrt{\frac{k_c m_h}{\mathbf{u}^T[m_h\mathbf{J}(\mathbf{q})\mathbf{M}(\mathbf{q})^{-1}\mathbf{J}^T(\mathbf{q}) + \mathbf{I}_{3\times3}]\mathbf{u}}} \tag{23}$$

According to [21], [22], the safe contact force and pressure limits that different regions of the human body can withstand under specific damping and stiffness conditions are summarized in Table I.

Considering a head-on collision between a human and a moving robotic arm along the same straight line but in opposite directions, we treat the combined system as a single entity $m_{\max} = \max(m_h, m_r)$. The total kinetic energy of the system is then given by:

$$K_n \le \frac{1}{2}m_{\max}v_h^2 + \frac{1}{2}m_{\max}v_r^2 = \frac{1}{2}m_{\max}v_{\text{rel}}^2 + m_{\max}v_h v_r \tag{24}$$

Furthermore, the energy states before and after the collision can be related. The system's safety energy limit before the collision,

Fig. 7. Hardware Configuration of the Mobile Manipulator.

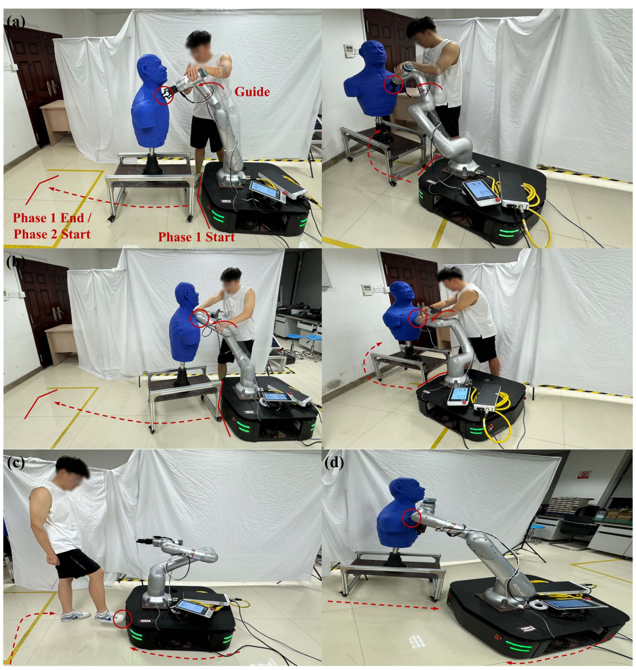

Fig. 8. Real-world experimental scenarios. (a-b) Intentional contact-guided tasks, where continuous force is applied via the end-effector and elbow joint, respectively, to guide the robot in a collaborative task involving pushing a mannequin. (c-d) Unintentional collision scenarios used to evaluate safety responses during dynamic tasks involving collisions between a human foot and a high-inertia platform, as well as unexpected collisions with the manipulator.

$K_{c,n}$, must be greater than or equal to the sum of the residual kinetic energy after the collision, $K_{c,n+1}$, and the energy dissipated or transformed during the collision process, E_{loss}. The maximum energy converted during the collision is related to the impact force and can be expressed as $E_{\text{loss}} \propto F_{\text{imp}}^2/k_c$.

Based on this principle, and in conjunction with equations (24) and (21), we can establish a conservative energy inequality that connects the pre-collision energy to the collision parameters and post-collision state:

$$K_{c,n} \geq \frac{F_{\text{imp}}^2}{2m_{\text{max}}k_c} + m_{\text{max}}v_h v_r \leq \frac{m_{\text{max}}F_{\text{imp}}^2}{m_h m_r k_c} + K_{c,n+1} \quad (25)$$

This inequality indicates that the energy loss caused by the collision must not exceed a stable upper bound. Assuming a collision occurs between the robotic arm and the human at time t, we establish the following risk quantification law:

Theorem 3 (Risk Quantification Law): The collision risk can be quantified by the Danger Index $f_D(t)$, defined as:

$$f_D(t) = \frac{m_{\text{max}}^2 F_{\text{imp}}^2}{m_h m_r k_c} \quad (26)$$

This unified metric provides a physically grounded measure of collision severity. By substituting the expression for impact force, the index simplifies to $f_D(t) = m_{\text{max}}^2 v_{\text{rel}}^2/(m_h + m_r)$. This reveals that the Danger Index captures the fundamental trade-off between the destabilizing effect of the system's dominant mass (the m_{max}^2 term) and the stabilizing, energy-absorbing capacity of the total combined mass (the $m_h + m_r$ term). As a continuous and monotonic function of impact force, it serves as a reliable indicator of injury risk.

When the Danger Index exceeds a predefined threshold, the system enters a hazardous state, reflecting the severity of potential injury to be mitigated, as illustrated in Fig. 4.

IV. Experiments

A. Benchmark Controller

To validate the effectiveness of the proposed method, we conducted a series of experiments in both simulated and real-world environments and benchmarked it against two representative controllers.

1) *Fixed-Impedance (FI) Control:* This controller uses a set of fixed low-impedance parameters throughout the entire task. It represents a fundamental passive compliance safety strategy and is a common baseline for evaluating the performance of active safety control.

2) *Bounded Energy Collision (BEC) Control:* This method [4] limits the total kinetic energy of the system within a predefined safety boundary by adjusting a global damping term. It is a SOTA benchmark for managing collision energy.

B. Gazebo Simulation

To this end, we designed four challenging scenarios in Gazebo: a frontal collision between the operator's hand and the robot's end-effector, a lateral collision between the operator's body and the robot's elbow joint, a collision between the operator's foot and a high-inertia moving platform, and a sudden obstacle appearing along the robot's path, as shown in Fig. 5. To ensure reliability, 30 collision experiments were conducted for each scenario, and the mean and standard deviation of the peak collision forces are summarized in Table II, clearly illustrating the comparative outcomes.

The statistical comparison in Fig. 6(d) further highlights this performance advantage. Taking the end-effector collision scenario in Table II as an example, our method produced a peak force of only 40.1 N, representing a 58.1% reduction compared to BEC (95.8 N) and a 77.1% reduction compared to the basic

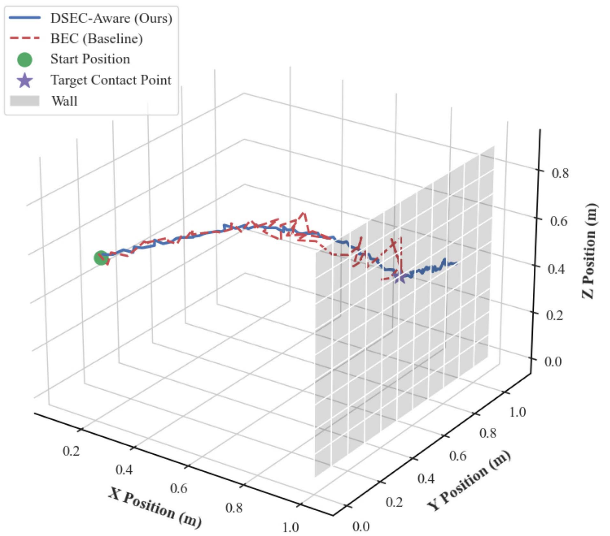

Fig. 9. Trajectory comparison between the DSEC-Aware and BEC controllers during the guidance task.

TABLE III
PERFORMANCE COMPARISON OF THE TWO CONTROLLERS IN THE REAL WORLD

Task Type	Trial	Metric	BEC	DSEC-Aware (Ours)	Improvement
Guidance Task	50	Completion Time (s)	15.6 $\pm$ 2.1	**8.2 $\pm$ 0.5**	**47.40%**
	50	Trajectory Smoothness	Low	**High**	**Significant**
	50	Controllable Force (N)	8.3 $\pm$ 1.5	**15.1 $\pm$ 1.1**	**45.03%**
Collision Test	50	Peak Impact Force (N)	95.8 $\pm$ 8.1	**40.2 $\pm$ 4.6**	**58.04%**
	50	Peak Danger Index	/	**15 $\pm$ 1.4**	/

FI (175.2 N). Similar significant improvements were observed in all other scenarios.

As shown in Fig. 6(e) and (f), all controllers adjust velocity upon collision, yet our method exhibits the smoothest and most stable response, dissipating energy effectively without oscillations or abrupt stops. The force–time curves in Fig. 6(a)–(c) further demonstrate that DSEC-Aware consistently achieves the lowest peak collision forces. In contrast, the FI controller generates the largest impacts due to the absence of adaptive impedance, while BEC mitigates impacts partially. By applying damping selectively along critical directions, DSEC-Aware attains superior suppression while preserving motion in safe directions.

C. Real-World Experiment

The physical experiments were conducted on a mobile manipulation platform (see Fig. 7) comprising a Ridgeback omnidirectional chassis and a 6-DOF LUXAI manipulator. The system integrates proprioceptive sensors for real-time joint feedback and fuses IMU data with wheel odometry for localization. A unified control architecture runs on an onboard PC with Ubuntu 20.04 and ROS Noetic, while an auxiliary PC converts joystick inputs via Bluetooth into ROS commands for intuitive task guidance.

To verify the practical applicability of the proposed method, a series of representative physical human–robot interaction tasks were conducted. First, a collaborative guidance task was designed to assess controller compliance and controllability, where a volunteer guided the robot to push a wheeled dummy precisely toward a target position. This task comprised two phases: comparison with the benchmark BEC controller and evaluation under sustained contact and force control conditions, as shown in Fig. 8(a) and (b).

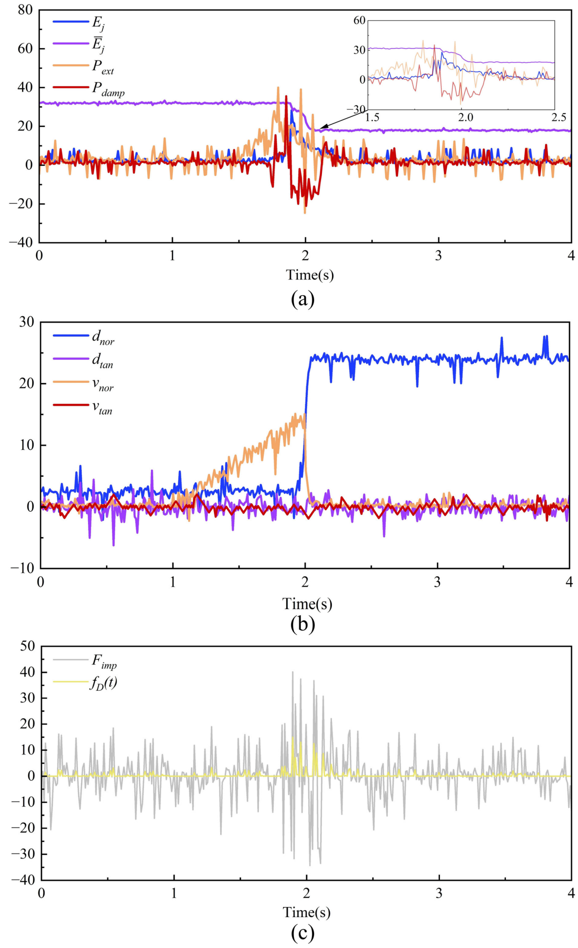

Fig. 10. Internal States of the DSEC-Aware Controller During Real-World Interaction Tasks. (a) Dissipated power constrains the kinetic energy within a safe boundary. (b) Directional damping selectively suppresses normal velocity. (c) The DI evaluation remains stably low despite contact force fluctuations.

1) *Phase One:* A volunteer is asked to perform the dummy-pushing task by freely controlling the robot via pushing, pulling, or guiding the end-effector, using both the proposed DSEC-Aware controller and the BEC benchmark controller.

2) *Phase Two:* Only the DSEC-Aware controller is used. A volunteer is required to maintain contact between the dummy and the wall, guiding the robot to push the dummy horizontally along the wall.

Building on this, we further designed two unintentional collision scenarios to evaluate the safety response capability of the mobile manipulator. These included a collision between a human foot and the high-inertia mobile chassis in a dynamic scenario, as well as unintended contact with the mobile manipulator. Each scenario was tested 50 times, as shown in Fig. 8(c) and (d).

As shown in Fig. 9, the proposed DSEC-Aware controller markedly surpasses BEC in both task performance and interaction safety. It enables the mobile manipulator to follow a smooth, direct trajectory, allowing the volunteer to push the dummy precisely and maintain stable sliding after wall contact. In contrast, BEC's global damping causes sluggish motion with noticeable yawing and jitter. Quantitatively (Table III), DSEC-Aware reduces the average peak collision force to 40.2 N—58.04% lower than BEC's 95.8 N—while shortening task time by 47.4%. It also lowers impact forces and yields favorable danger index values in unintentional collisions.

Fig. 10 depicts the internal dynamics of the DSEC-Aware controller during interaction. As shown in Fig. 10(a), when the kinetic energy E_j nears its upper bound $\bar{E}_j$, the controller produces negative dissipative power Pdamp comparable to the external input P_{ext}, thereby keeping energy within safe limits. Meanwhile, the tangential velocity $v_{\tan}$ stays smooth under zero tangential damping $d_{\tan}$, ensuring efficiency, while normal damping d_{nor} is activated once v_{nor} becomes hazardous (Fig. 10(b)), ensuring safety. Finally, Fig. 10(c) shows that although contact force F_{imp} fluctuates, the danger index $f_D(t)$ remains low and stable, confirming effective risk regulation.

V. Conclusions and Future Work

This letter introduced the DSEC-Aware framework, a comprehensive solution for post-collision safety in HRC that addresses the critical limitations of conventional methods. By replacing geometric proxies with direct energy constraints, substituting global damping with a selective, optimal intervention, and advancing from partial to holistic risk assessment via a multidimensional Danger Index, our approach establishes a more physically grounded safety paradigm. Experimental validation confirms its effectiveness: compared to the SOTA BEC method, the framework reduces peak collision forces by approximately 58.04% while simultaneously enhancing task efficiency and trajectory smoothness. By ensuring safety without unduly compromising performance, this work offers a significant step towards more practical and reliable physical human-robot collaboration.

Future research will focus on integrating advanced perception systems and deep learning techniques to achieve predictive collision avoidance, shifting the system from reactive response to feedforward safety control. Furthermore, we aim to extend the framework to multi-robot collaboration scenarios and develop adaptive learning mechanisms that personalize safety parameters based on individual operator preferences, thereby achieving a higher level of safety in HRC.

References

[1] S. Robla-Gómez, V. M. Becerra, J. R. Llata, E. González-Sarabia, C. Torre-Ferrero, and J. Pérez-Oria, "Working together: A review on safe human-robot collaboration in industrial environments," *IEEE Access*, vol. 5, pp. 26754–26773, 2017.

[2] Y. Pi, S. Feng, Q. Chen, and K. Wu, "Adaptive admittance control for active compliant under dynamic motion," in *Proc. 10th Int. Conf. Electr. Eng., Control Robot.*, 2024, pp. 140–145.

[3] X. Zhao, S. Han, B. Tao, Z. Yin, and H. Ding, "Model-based actor-critic learning of robotic impedance control in complex interactive environment," *IEEE Trans. Ind. Electron.*, vol. 69, no. 12, pp. 13225–13235, Dec. 2022.

[4] J. Sandoval et al., "Energy regulation of torque-driven robot manipulators in joint space," *J. Franklin Inst.*, vol. 359, no. 4, pp. 1427–1456, 2022.

[5] D. I. Park et al., "Variable passive compliant device for the robotic assembly," in *Proc. 14th Int. Conf. Ubiquitous Robots Ambient Intell.*, 2017, pp. 753–754.

[6] P. Kormushev et al., "Learning to exploit passive compliant for energy-efficient gait generation on a compliant humanoid," *Auton. Robots*, vol. 43, pp. 79–95, 2019.

[7] L. C. Zeng, "Research on flexible control method for industrial robot surface tracking," Ph.D. Dissertation, Xiangtan Univ., Xiangtan, China, 2021.

[8] X. L. Zhang et al., "A flexible robotic arm design based on series elastic actuator," *Robot*, vol. 38, no. 4, pp. 385–394, 2016, doi: 10.13973/j.cnki.robot.2016.0385.

[9] S. S. Bi et al., "Variable stiffness actuators: A review of the structural research," *J. Mech. Eng.*, vol. 54, no. 13, pp. 34–46, 2018, doi: 10.3901/JME.2018.13.034.

[10] E. Koco, D. Mirkovic, and Z. Kovačić, "Hybrid compliant control for locomotion of electrically actuated quadruped robot," *J. Intell. Robot. Syst.*, vol. 94, pp. 537–563, 2019.

[11] W. Wang, R. N. K. Loh, and E. Y. Gu, "Passive compliant versus active compliant in robot-based automated assembly systems," *Ind. Robot.: Int. J.*, vol. 25, no. 1, pp. 48–57, 1998.

[12] X. Liu et al., "A dynamic behavior control framework for physical human-robot interaction," *J. Intell. Robot. Syst.*, vol. 101, no. 1, 2021, Art. no. 14, doi: 10.1007/s10846-020-01286-x.

[13] K. S. Kim, T. Llado, and L. Sentis, "Full-body collision detection and reaction with omnidirectional mobile platforms: A step towards safe human-robot interaction," *Auton. Robots*, vol. 40, no. 2, pp. 325–341, 2016.

[14] C. Baspinar, "Robust position/force control of constrained flexible joint robots with constraint uncertainties," *J. Intell. Robot. Syst.*, vol. 100, no. 3, pp. 945–954, 2020.

[15] R. Rossi, M. P. Polverini, A. M. Zanchettin, and P. Rocco, "A pre-collision control strategy for human-robot interaction based on dissipated energy in potential inelastic impacts," in *Proc. IEEE/RSJ Int. Conf. Intell. Robots Syst.*, 2015, pp. 26–31.

[16] W. He, C. Xue, X. Yu, Z. Li, and C. Yang, "Admittance-based controller design for physical human-robot interaction in the constrained task space," *IEEE Trans. Autom. Sci. Eng.*, vol. 17, no. 4, pp. 1937–1949, Oct. 2020.

[17] M. Pan et al., "Collision risk assessment and automatic obstacle avoidance strategy for teleoperation robots," *Comput. Ind. Eng.*, vol. 169, 2022, Art. no. 108275.

[18] X. Zhang, Z. Zhong, W. Guan, M. Pan, and K. Liang, "Collision-risk assessment model for teleoperation robots considering acceleration," *IEEE Access*, vol. 12, pp. 101756–101766, 2024.

[19] I. Kostavelis, L. Nalpantidis, and A. Gasteratos, "Collision risk assessment for autonomous robots by offline traversability learning," *Robot. Auton. Syst.*, vol. 60, no. 11, pp. 1367–1376, 2012.

[20] M. Laffranchi, N. G. Tsagarakis, and D. G. Caldwell, "Safe human robot interaction via energy regulation control," in *Proc. IEEE/RSJ Int. Conf. Intell. Robots Syst.*, 2009, pp. 35–41.

[21] F. Ferraguti, M. Bertuletti, C. T. Landi, M. Bonfè, C. Fantuzzi, and C. Secchi, "A control barrier function approach for maximizing performance while fulfilling to ISO/TS 15066 regulations," *IEEE Robot. Autom. Lett.*, vol. 5, no. 4, pp. 5921–5928, Oct. 2020.

[22] X. Zhang, T. Sun, and D. Deng, "Neural approximation-based adaptive variable impedance control of robots," *Trans. Inst. Meas. Control*, vol. 42, no. 13, pp. 2589–2598, 2020.

[23] S. Kucuk and Z. Bingul, *Robot Kinematics: Forward and Inverse Kinematics*. London, U.K.: INTECH Open Access Publisher, 2006.

[24] S. D. Lee, B. S. Kim, and J. B. Song, "Human-robot collision model with effective mass and manipulability for design of a spatial manipulator," *Adv. Robot.*, vol. 27, no. 3, pp. 189–198, 2013.

[25] G. Jeanneau, V. Bégoc, and S. Briot, "A reduced mass-spring-mass-model of compliant robots dedicated to the evaluation of impact forces," *J. Mech. Robot.*, vol. 16, no. 4, 2024, Art. no. 041003.

[26] F. Dimeas and N. Aspragathos, "Online stability in human-robot cooperation with admittance control," *IEEE Trans. Haptics*, vol. 9, no. 2, pp. 267–278,Apr.-Jun. 2016.

[27] K. Garg et al., "Advances in the theory of control barrier functions: Addressing practical challenges in safe control synthesis for autonomous and robotic systems," *Annu. Rev. Control*, vol. 57, 2024, Art. no. 100945.

[28] R. Liu, R. Chen, A. Abuduweili, and C. Liu, "Proactive human-robot co-assembly: Leveraging human intention prediction and robust safe control," in *Proc. IEEE Conf. Control Technol. Appl.*, 2023, pp. 339–345.